Check for updates

Three-Dimensional Simulations of Subaerial Landslide-Generated Waves: Comparing OpenFOAM and FLOW-3D HYDRO Models

RAMTIN SABETI,[1] (iD) MOHAMMAD HEIDARZADEH,[1] ALESSANDRO ROMANO,[2,3] GABRIEL BARAJAS OJEDA,[3] and JAVIER L. LARA[3]

Abstract—The recent destructive landslide tsunamis, such as the 2018 Anak Krakatau event, were fresh reminders for developing validated three-dimensional numerical tools to accurately model landslide tsunamis and to predict their hazards. In this study, we perform Three-dimensional physical modelling of waves generated by subaerial solid-block landslides, and use the data to validate two numerical models: the commercial software FLOW-3D HYDRO and the open-source OpenFOAM package. These models are key representatives of the primary types of modelling tools—commercial and open-source—utilized by scientists and engineers in the field. This research is among a few studies on 3D physical and numerical models for landslide-generated waves, and it is the first time that the aforementioned two models are systematically compared. We show that the two models accurately reproduce the physical experiments and give similar performances in modelling landslide-generated waves. However, they apply different approaches, mechanisms and calibrations to deliver the tasks. It is found that the results of the two models are deviated by approximately 10% from one another. This guide helps engineers and scientists implement, calibrate, and validate these models for landslide-generated waves. The validity of this research is confined to solid-block subaerial landslides and their impact in the near-field zone.

Keywords: Tsunami, subaerial landslide, physical modelling, open FOAM, FLOW-3D HYDRO.

1. Introduction and Literature Review

Subaerial landslide-generated waves represent major threats to coastal areas and have resulted in destruction and casualties in several locations worldwide (Heller et al., 2016; Paris et al., 2021). Interest in landslide-generated tsunamis has risen in the last decade due to a number of devastating events, especially after the December 2018 Anak Krakatau tsunami which left a death toll of more than 450 people (Grilli et al., 2021; Heidarzadeh et al., 2020a). Another significant subaerial landslide tsunami occurred on 16 October 1963 in Vajont dam reservoir (Northern Italy), when an impulsive landslide-generated wave overtopped the dam, killing more than 2000 people (Heller & Spinneken, 2013; Panizzo et al., 2005). The largest tsunami run-up (524 m) was recorded in Lituya Bay landslide tsunami event in 1958 where it killed five people (Fritz et al., 2009).

To achieve a better understanding of subaerial landslide tsunamis, laboratory experiments have been performed using two- and three-dimensional (2D, 3D) set-ups (Bellotti & Romano, 2017; Di Risio et al., 2009; Fritz et al., 2004; Romano et al., 2013; Sabeti & Heidarzadeh, 2022a). Results of physical models are essential to shed light on the nonlinear physical phenomena involved. Furthermore, they can be used to validate numerical models (Fritz et al., 2009; Grilli & Watts, 2005; Liu et al., 2005; Takabatake et al., 2022). However, the complementary development of numerical tools for modelling of landslide-generated waves is inevitable, as these models could be employed to accelerate understanding the nature of the processes involved and predict the detailed outcomes in specific areas (Cremonesi et al. 2011). Due to the high flexibility of numerical models and their low costs in comparison to physical models, validated numerical models can be used to replicate actual events at a fair cost and time (e.g., Cecioni et al., 2011; Grilli et al., 2017; Heidarzadeh

[1] Department of Architecture and Civil Engineering, University of Bath, Bath BA2 7AY, UK. E-mail: rs3195@bath.ac.uk

[2] Engineering Department, Roma Tre University, Via Vito Volterra, 62, 00146 Rome, Italy.

[3] IHCantabria-Instituto de Hidráulica Ambiental de la Universidad de Cantabria, Santander, Spain.

et al., 2020b, 2022; Horrillo et al., 2013; Liu et al., 2005; Løvholt et al., 2005; Lynett & Liu, 2005).

Table 1 lists some of the existing numerical models for landslide tsunamis although the list is not exhaustive. Traditionally, Boussinesq-type models, and Shallow water equations have been used to simulate landslide tsunamis, among which are TWO-LAYER (Imamura and Imteaz,1995), LS3D (Ataie-Ashtiani & Najafi Jilani, 2007), GLOBOUSS (Løvholt et al., 2017), and BOUSSCLAW (Kim et al., 2017). Numerical models that solve Navier–Stokes equations showed good capability and reliability to simulate subaerial landslide-generated waves (Biscarini, 2010). Considering the high computational cost of solving the full version of Navier–Stokes equations, a set of methods such as RANS (Reynolds-averaged Navier–Stokes equations) are employed by some existing numerical models (Table 1), which provide an approximate averaged solution to the Navier–Stokes equations in combination with turbulent models (e.g., k–ε, k–ω). Multiphase flow models were used to simulate the complex dynamics of landslide-generated waves, including scenarios where the landslide mass is treated as granular material, as in the work by Lee and Huang (2021), or as a solid block (Abadie et al., 2010). Among the models listed in Table 1, FLOW-3D HYDRO and OpenFOAM solve Navier–Stokes equations with different approaches (e.g., solving the RANS by IHFOAM) (Paris et al., 2021; Rauter et al., 2022). They both offer a wide range of turbulent models (e.g., Large Eddy Simulation—LES, k–ε, k–ω model with Renormalization Group—RNG), and they both use the VOF (Volume of Fluid) method to track the water surface elevation. These similarities are one of the motivations of this study to compare the performance of these two models. Details of governing equations and numerical schemes are discussed in the following.

In this work, we apply two Computational Fluid Dynamic (CFD) frameworks, FLOW-3D HYDRO, and OpenFOAM to simulate waves generated by solid-block subaerial landslides in a 3D set-up. We calibrate and validate both numerical models using our physical experiments in a 3D wave tank and compare the performances of these models systematically. These two numerical models are selected among the existing CFD solvers because they have

been reported to provide valuable insights into landslide-generated waves (Kim et al., 2020; Romano et al., 2020a, b ; Sabeti & Heidarzadeh, 2022a). As there is no study to compare the performances of these two models (FLOW-3D HYDRO and Open-FOAM) with each other in reproducing landslide-generated waves, this study is conducted to offer such a comparison, which can be helpful for model selection in future research studies or industrial projects. In the realm of tsunami generation by subaerial landslides, the solid-block approach serves as an effective representative for scenarios where the landslide mass is more cohesive and rigid, rather than granular. This methodology is particularly relevant in cases such as the 2018 Anak Krakatau or 1963 Vajont landslides, where the landslide's nature aligns closely with the characteristics simulated by a solid-block model (Zaniboni & Tinti, 2014; Heidarzadeh et al., 2020a, 2020b).

The objectives of this research are: (i) To provide a detailed implementation and calibration for simulating solid-block subaerial landslide-generated waves using FLOW-3D HYDRO and OpenFOAM, and (ii) To compare the performance of these two numerical models based on three criteria: free surface elevation of the landslide-generated waves, capabilities of the models in simulating 3D features of the waves in the near-field, velocity fields, and velocity variations at different locations. The innovations of this study are twofold: firstly, it is a 3D study involving physical and numerical modelling and thus the data can be useful for other studies, and secondly, it compares the performance of two popular CFD models in modelling landslide-generated waves for the first time. The validated models such as those reported in this study and comparison of their performances can be useful for engineers and scientists addressing landslide tsunami hazards worldwide.

2. Data and Methods

2.1. Physical Modelling

To validate our numerical models, a series of three-dimensional physical experiments were carried out at the Hydraulic Laboratory of the Brunel

Table 1

Some of the existing numerical models for simulating landslide-generated waves

Numerical models	Approach	Developer
FLOW-3D HYDRO	This CFD package solves Navier–Stokes equations using finite-difference and finite volume approximations, along with Volume of Fluid (VOF) method for tracking the free surface	Flow Science, Inc. (https://www.flow3d.com/)
MIKE 21	This model is based on the numerical solution of 2D and 3D incompressible RANS equations subject to the assumptions of Boussinesq and hydrostatic pressure	Danish Hydraulic Institute (DHI) (https://www.mikepoweredbydhi.com/products/mike-21-3)
OpenFOAM (IHFOAM solver)	IHFOAM is a newly developed 3D numerical two-phase flow solver. Its core is based on OpenFOAM®. IHFOAM can also solve two-phase flow within porous media using RANS/VARANS equations	IHCantabria research institute (https://ihfoam.ihcantabria.com/)
NHWAVE	NHWAVE is a 3D shock-capturing non-Hydrostatic model which solves the incompressible Navier–Stokes equations in terrain and surface-following sigma coordinates	Kirby et al. (2022) (https://sites.google.com/site/gangfma/nhwave, https://github.com/JimKirby/NHWAVE)
GLOBOUSS	GloBouss is a depth-averaged model based on the standard Boussinesq equations including higher order dispersion terms, Coriolis terms, and numerical hydrostatic correction terms	Løvholt et al. (2022) (https://www.duo.uio.no/handle/10852/10184)
BOUSSCLAW	BoussClaw is a new hybrid Boussinesq type model which is an extension of the GeoClaw model. It employs a hybrid of finite volume and finite difference methods to solve Boussinesq equations	Clawpack Development Team (http://www.clawpack.org/) Kim et al. (2017)
THETIS-MUI	THETIS is a multi-fluid Navier–Stokes solver which can be considered a one-fluid model as only one velocity is defined at each point of the mesh and there is no mixing between the three considered fluids (water, air, and slide). It applies VOF method	TREFLE department of the I2M Laboratory at Bordeaux, France (https://www.i2m.u-bordeaux.fr/en)
LS3D	A 2D depth-integrated numerical model which applies a fourth-order Boussinesq approximation for an arbitrary time-variable bottom boundary	Ataie-Ashtiani and Najafi Jilani (2007)
LYNETT- Mild-Slope Equation (MSE)	MSE is a depth-integrated version of the Laplace equation operating under the assumption of inviscid flow and mildly varying bottom slopes	Lynett and Martinez (2012)
Tsunami 3D	A simplified 3D Navier–Stokes model for two fluids (water and landslide material) using VOF for tracking of water surface	Horrillo et al. (2013) Kim et al. (2020)
(Cornell Multi-grid Coupled Tsunami Mode (COMCOT)	COMCOT adopts explicit staggered leap-frog finite difference schemes to solve Shallow Water Equations in both Spherical and Cartesian Coordinates	Liu et al. (1998); Wang and Liu (2006)
TWO-LAYER	A mathematical model for a two-layer flow along a non-horizontal bottom. Conservation of mass and momentum equations are depth integrated in each layer, and nonlinear kinematic and dynamic conditions are specified at the free surface and at the interface between fluids	Imamura and Imteaz (1995)

University London (UK) in a 3D wave tank 2.40 m long, 2.60 m wide, and 0.60 m high (Figs. 1 and 2). To mitigate experimental errors and enhance the reliability of our results, each physical experiment was conducted three times. The reported data in the manuscript reflects the average of these three trials, assuming no anomalous outliers, thus ensuring an accurate reflection of the experimental tests. One

experiment was used for validation of our numerical models. The slope angle (α) and water depth (h) were 45° and 0.246 m, respectively for this experiment. The movement of the sliding mass was recorded by a digital camera with a sampling frequency of 120 frames per second, which was used to calculate the slide impact velocity (v_s). The travel distance (D), defined as the distance from the toe of the sliding
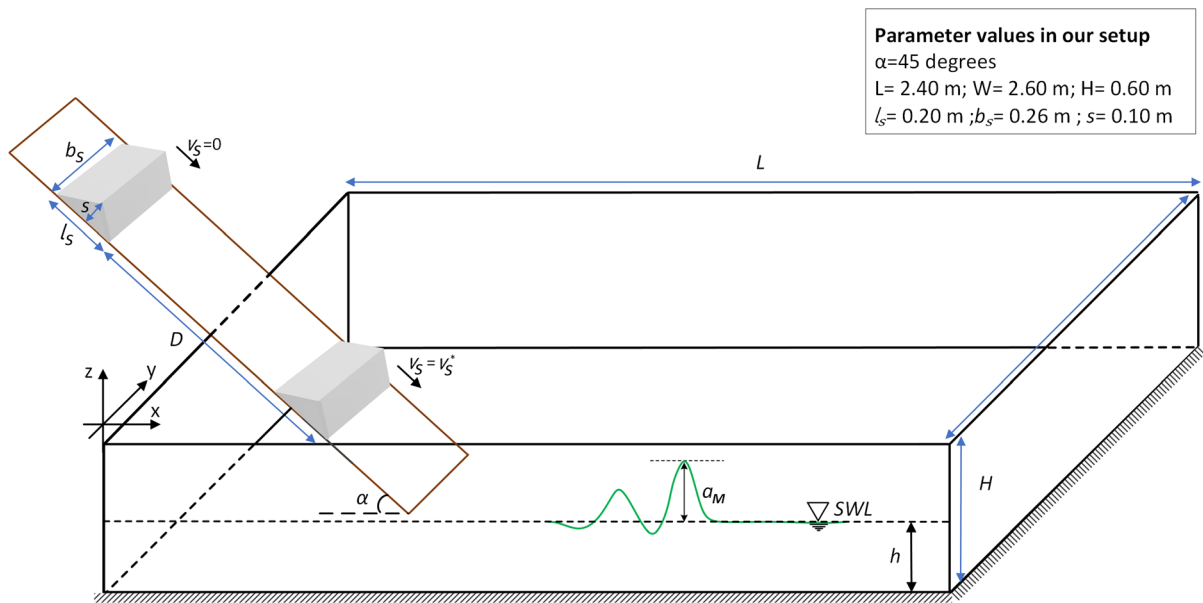
Parameter values in our setup
α=45 degrees
L= 2.40 m; W= 2.60 m; H= 0.60 m
l_s= 0.20 m ; b_s= 0.26 m ; s= 0.10 m

Figure 1
The geometrical and kinematic parameters of a subaerial landslide tsunami. Parameters are: h, water depth; a_M, maximum wave amplitude; α, slope angle; v_s, slide velocity; l_s, length of landslide; b_s, width of landslide; s, thickness of landslide; SWL, still water level; D, travel distance (the distance from the toe of the sliding mass to the water surface); L, length of the wave tank; and W, width of the wave tank and H, is the hight of the wave tank

mass to the water surface, was D=0.045 m. The material of the solid block used in our study was concrete with a density of 2600 kg/m³. Table 2 provides detailed information on the dimensions and kinematics of this solid block used in our physical experiments.

We took scale effects into account during physical experiments by considering the study by Heller et al. (2008) who proposed a criterion for avoiding scale effects. Heller et al. (2008) stated that the scale effects can be negligible as long as the Weber number ($W = \rho g h^2/\sigma$; where σ is surface tension coefficient) is greater than 5.0×10^3 and the Reynolds number ($R = g^{0.5} h^{1.5}/v$; where v is kinematic viscosity) is greater than 3.0×10^5 or water depth (h) is approximately above 0.20 m. Considering the water temperature of approximately 20 °C during our experiments, the kinematic viscosity (v) and surface tension coefficient (σ) of water become 1.01×10^{-6} m²/s and 0.073 N/m, respectively. Therefore, the Reynolds and Weber numbers were as $R = 3.8 \times 10^5$ and $W = 8.1 \times 10^5$, indicating that the scale effect can be insignificant in our experiments. To record the

waves, we used a twin wire wave gauge provided by HR Wallingford (https://equipit.hrwallingford.com). This wave gauge was placed at $X = 1.03$ m, $Y = 1.21$ m based on the coordinate system shown in Fig. 2a.

2.2. Numerical Simulations

The numerical simulations in this work were performed employing two CFD packages FLOW-3D HYDRO, and OpenFOAM which have been widely used in industry and academia (e.g., Bayon et al., 2016; Jasak, 2009; Rauter et al., 2021; Romano et al., 2020a, b; Yin et al., 2015).

2.2.1 Governing Equations and Turbulent Models

2.2.1.1 FLOW-3D HYDRO The FLOW-3D HYDRO solver is based on the fundamental law of mass, momentum and energy conservation. To estimate the influence of turbulent fluctuations on the flow quantities, it is expressed by adding the diffusion
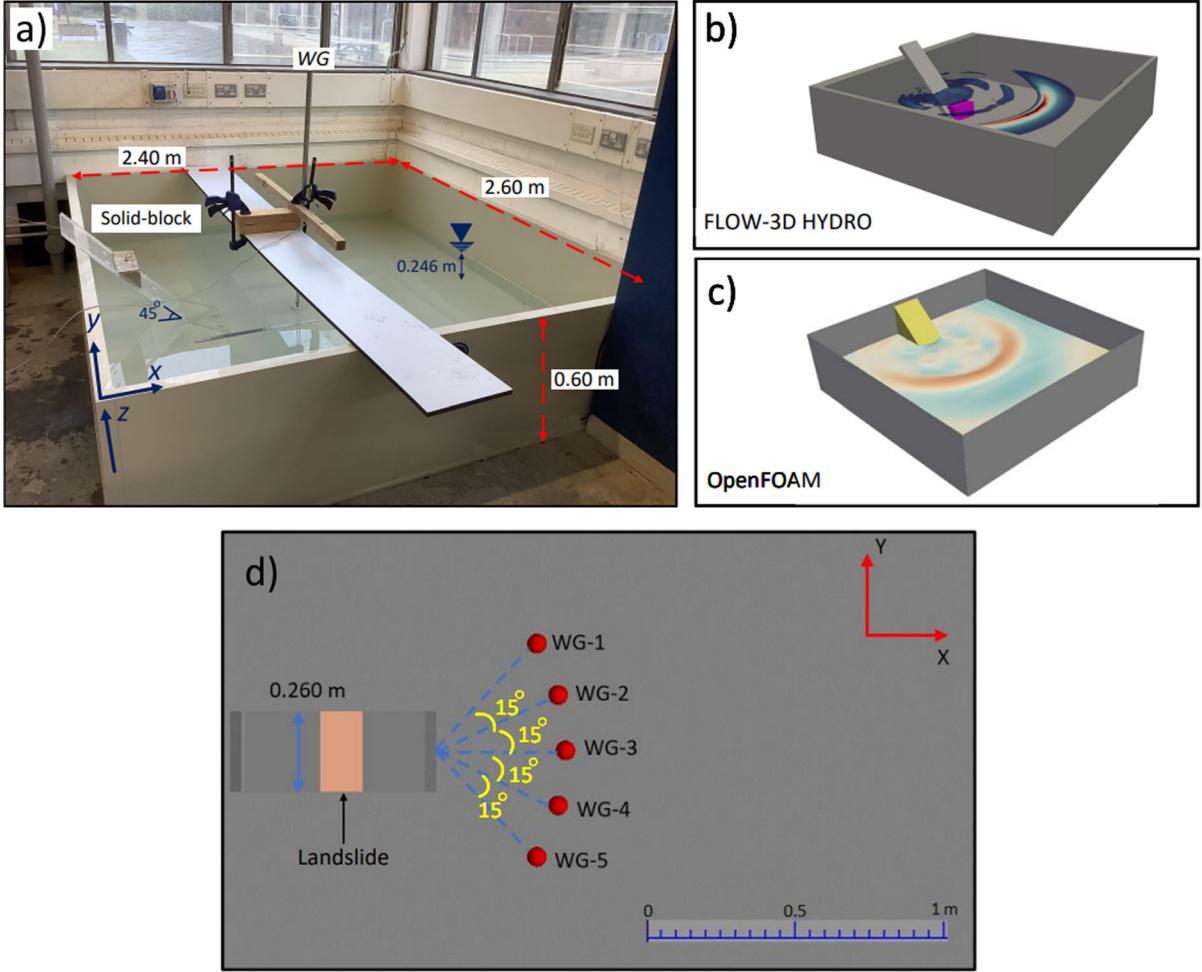
Figure 2

a Wave tank setup of the physical experiments of this study. **b** Numerical simulation setup for the FLOW-3D HYDRO Model. **c** The numerical set-up for the OpenFOAM model. The location of the physical wave gauge (represented by numerical gauge WG-3 in the numerical simulations) is at $X = 1.03$ m, $Y = 1.21$ m, and $Z = 0.046$ m. **d** Top view showing the locations of numerical wave gauges (WG-1, WG-2, WG-3, WG-4, WG-5)

terms in the following mass continuity and momentum transport equations:

$$V_F \frac{\partial \rho}{\partial t} + \frac{\partial}{\partial x}(\rho u A_x) + \xi \frac{\rho u A_x}{x} = R_{DIF} + R_{SOR} \quad (1)$$

$$R_{DIF} = \frac{\partial}{\partial x}\left(U_\rho A_x \frac{\partial \rho}{\partial x}\right) + \xi \frac{U_\rho A_x}{x} \frac{\partial \rho}{\partial x} \quad (2)$$

$$\frac{R_{SOR}}{\rho} = \frac{\partial}{\partial x}(u A_x) + \xi \frac{u A_x}{x} \quad (3)$$

Equation (1) is the general mass continuity equation, where u is fluid velocity in the Cartesian coordinate directions (x), A_x is the fractional area open to flow in the x direction, V_F is the fractional volume open to flow, ρ is the fluid density, R and ξ are coefficients that depend on the choice of the coordinate system. When Cartesian coordinates are used, R is set to unity and ξ is set to zero. R_{DIF} and R_{SOR} are the turbulent diffusion and density source terms, respectively. $U_\rho = S_c \mu^*/\rho$, in which S_c is the turbulent Schmidt number, μ^* is the dynamic viscosity, and ρ is fluid density. R_{SOR} is applied to model mass injection through porous obstacle surfaces.

Table 2

Geometrical and kinematic information of the sliding mass used for physical experiments in this study

Parameter, unit	Value/type
Slide width (b_s), m	0.26
Slide length (l_s), m	0.20
Slide thickness (s), m	0.10
Slide volume (V), m³	2.60×10^{-3}
Specific gravity, (γ_s)	2.60
Slide weight (m_s), kg	6.86
Slide impact velocity (v_s), m/s	1.84
Slide Froude number (F_r)	1.18
Material	Concrete

The slide Froude number (F_r) is calculated by using the following equation: $F_r = v_s/\sqrt{gh}$; here v_s is slide impact velocity, g is gravitational acceleration, and h is water depth ($h = 0.246$ m in our physical experiments)

The 3D equations of motion are solved with the following Navier–Stokes equations with some additional terms:

$$
\frac{\partial u}{\partial t} + \frac{1}{V_F}\left\{ uA_x \frac{\partial u}{\partial x} \right\} - \xi \frac{A_y v^2}{x V_F}
$$
$$
= -\frac{1}{\rho}\frac{\partial p}{\partial x} + G_x + f_x - b_x - \frac{R_{SOR}}{\rho V_F}(u) \qquad (4)
$$

where t is time, G_x is accelerations due to gravity, f_x is viscous accelerations, and b_x is the flow losses in porous media.

According to Flow Science (2022), FLOW-3D HYDRO's turbulence models differ slightly from other formulations by generalizing the turbulence production with buoyancy forces at non-inertial accelerations and by including the influence of fractional areas/volumes of the FAVOR method (Fractional Area-Volume Obstacle Representation) method. Here we use k–ω model for turbulence modelling. The k–ω model demonstrates enhanced performance over the k-ε and Renormalization-Group (RNG) methods in simulating flows near wall boundaries. Also, for scenarios involving pressure changes that align with the flow direction, the k–ω model provides more accurate simulations, effectively capturing the effects of these pressure variations on the flow (Flow Science, 2022). The equations for turbulence kinetic energy are

formulated as below based on Wilcox's k–ω model (Flow Science, 2022):

$$
\frac{\partial k_T}{\partial t} + \frac{1}{V_F}\left\{ uA_x \frac{\partial k_T}{\partial x} \right\} = P_T + G_T + Diff_{K_T} - \beta^* \rho\omega
$$
$$(5)$$

where k_T is turbulent kinetic energy, P_T is the turbulent kinetic energy production, $Diff_{K_T}$ is diffusion of turbulent kinetic energy, G_T is buoyancy production, $\beta^* = 0.09$ is closure coefficient, and ω is turbulent frequency.

2.2.1.2 OpenFOAM For the simulations conducted in this study, OpenFOAM utilizes the Volume-Averaged RANS equations (VARANS) to enable the representation of flow within porous material, treated as a continuous medium. The momentum equation incorporates supplementary terms to accommodate frictional forces from the porous media. The mass and momentum conservation equations are linked to the VOF equation (Jesus et al., 2012) and are expressed as follows:

$$
\frac{\partial \overline{u}_i}{\partial x_i n} = 0 \qquad (6)
$$

$$
(1+c)\frac{\partial \rho \overline{u}_i}{\partial t n} + \frac{\overline{u}_i \partial \rho \overline{u}_i}{\partial x_j n} = -g_j x_j \frac{\partial \rho}{\partial x_i} - \frac{\partial P^*}{\partial x_i} - f_{\sigma i}
$$
$$
- \frac{\partial}{\partial x_j}\mu_{eff}\left(\frac{\partial \rho \overline{u}_i}{\partial x_j n} + \frac{\partial \rho \overline{u}_i}{\partial x_i n}\right)
$$
$$
- A\overline{u}_i - B|\overline{u}_i|\overline{u}_i
$$
$$(7)$$

$$
\frac{\partial \tau}{\partial_t} + \frac{\partial \overline{u}_i \tau}{\partial x_i n} + \frac{\partial \overline{u}_{ic}\tau(1-\tau)}{\partial x_i n} = 0 \qquad (8)
$$

where the gravitational acceleration components are denoted by g_j. The term $\overline{u}_i = \frac{1}{V_f}\int_{V_f}^0 u_j dV$ represents the volume averaged ensemble averaged velocity (or Darcy velocity) component, V_f is the fluid volume contained in the average volume V, τ is the surface tension constant (assumed to be 1 for the water phase and 0 for the air phase), and $f_{\sigma i}$ is surface tension, defined as $f_{\sigma i} = \sigma\kappa\frac{\partial \alpha}{\partial x_i}$, where σ (N/m) is the surface tension constant and κ (1/m) is the curvature (Brackbill et al., 1992). μ_{eff} is the effective dynamic viscosity that is defined as $\mu_{eff} = \mu + \rho v_t$ and takes into account the dynamic molecular (μ) and the turbulent viscosity effects (ρv_t). v_t is eddy viscosity,
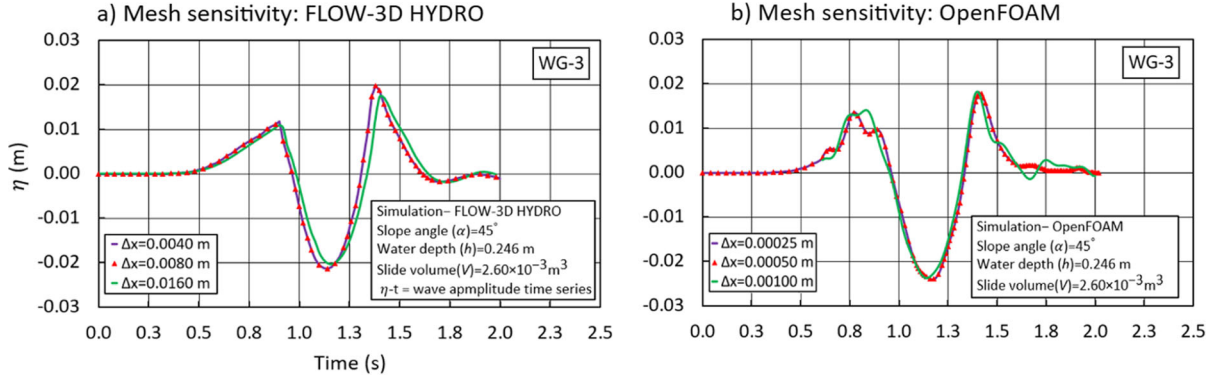
Figure 3
a, b Sensitivity of numerical simulations to the sizes of the mesh (Δx) for FLOW-3D HYDRO, and OpenFOAM, respectively. The location of the wave gauge 3 (WG-3) is at $X = 1.03$ m, $Y = 1.21$ m, and $Z = -0.55$ m (see Fig. 2d)
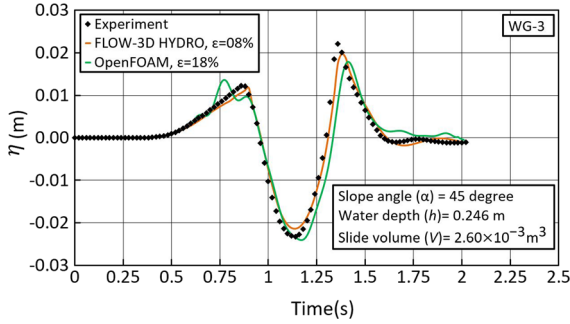

Figure 4
Validation of the simulated waves (brown line for FLOW-3D HYDRO and green line for OpenFOAM) using the laboratory-measured waves (black solid diamonds). This physical experiment was conducted for wave gauge 3 (WG-3) located at $X = 1.03$ m, $Y = 1.21$ m, and $Z = -0.55$ m (see Fig. 2d). Here, ε shows the errors between simulations and actual physical measurements using Eq. (13)

which is provided by the turbulence closure model. n is the porosity, defined as the volume of voids over total volume, and $P^* = \frac{1}{V_f} \int_{\partial V_f}^{0} P^* dS$ is the ensemble averaged pressure in excess of hydrostatic pressure. The coefficient A accounts for the frictional force induced by laminar Darcy-type flow, B considers the frictional force under turbulent flow conditions, and c accounts for the added mass. These coefficients (A,B, and c) are defined based on the work of Engelund (1953) and later modified by Van Gent (1995) as given below:

$$A = a \frac{(1 - n)^2 \mu}{n^3 D_{50}^2} \tag{9}$$

$$B = b(1 + \frac{7.5}{KC}) \frac{(1 - n)\rho}{n^3 D_{50}} \tag{10}$$

$$c = \gamma \frac{1 - n}{n} \tag{11}$$

where D_{50} is the mean nominal diameter of the porous material, KC is the Keulegan–Carpenter number, a and b are empirical nondimensional coefficients (see Lara et al., 2011; Losada et al., 2016) and $\gamma = 0.34$ is a nondimensional parameter as proposed by Van Gent (1995). The k-ω Shear Stress Transport (SST) turbulence is employed to capture the effect of turbulent flow conditions (Zhang & Zhang, 2023) with the enhancement proposed by Larsen and Fuhrman (2018) for the over-production of turbulence beneath surface waves. Boundary layers are modelled with wall functions. The reader is referred to Larsen and Fuhrman (2018) for descriptions, validations, and discussions of the stabilized turbulence models.

2.2.2 FLOW-3D HYDRO Simulation Procedure

In our specific case in this study, FLOW-3D HYDRO utilizes the finite-volume method to numerically solve the equations described in the previous Sect. 2.2.1.1, ensuring a high level of accuracy in the computational modelling. The use of structured rectangular grids in FLOW-3D HYDRO offers the

advantages of easier development of numerical methods, greater transparency in their relation to physical problems, and enhanced accuracy and stability of numerical solutions. (Flow Science, 2022). Curved obstacles, wall boundaries, or other geometric features are embedded in the mesh by defining the fractional face areas and fractional volumes of the cells that are open to flow (the FAVOR method). The VOF method is employed in FLOW-3D HYDRO for accurate capturing of the free-surface dynamics (Hirt and Nichols 1981). This approach then is upgraded to method of the TruVOF which is a split Lagrangian method that typically produces lower cumulative

volume error than the alternative methods (Flow Science, 2022).

For numerical simulation using FLOW-3D HYDRO, the entire flow domain was 2.60 m wide, 0.60 m deep and 2.50 m long (Fig. 2b). The specific gravity (γ_s) for solid blocks was set to 2.60 in our model, aligning closely with the density of the actual sliding mass, which was approximately determined in our physical experiments. The fluid medium was modelled as water with a density of 1000 kg/m^3 at 20 °C. A uniform grid comprising of one single mesh plane was applied with a grid size of 0.005 m. The top, front and back of the mesh areas were defined as
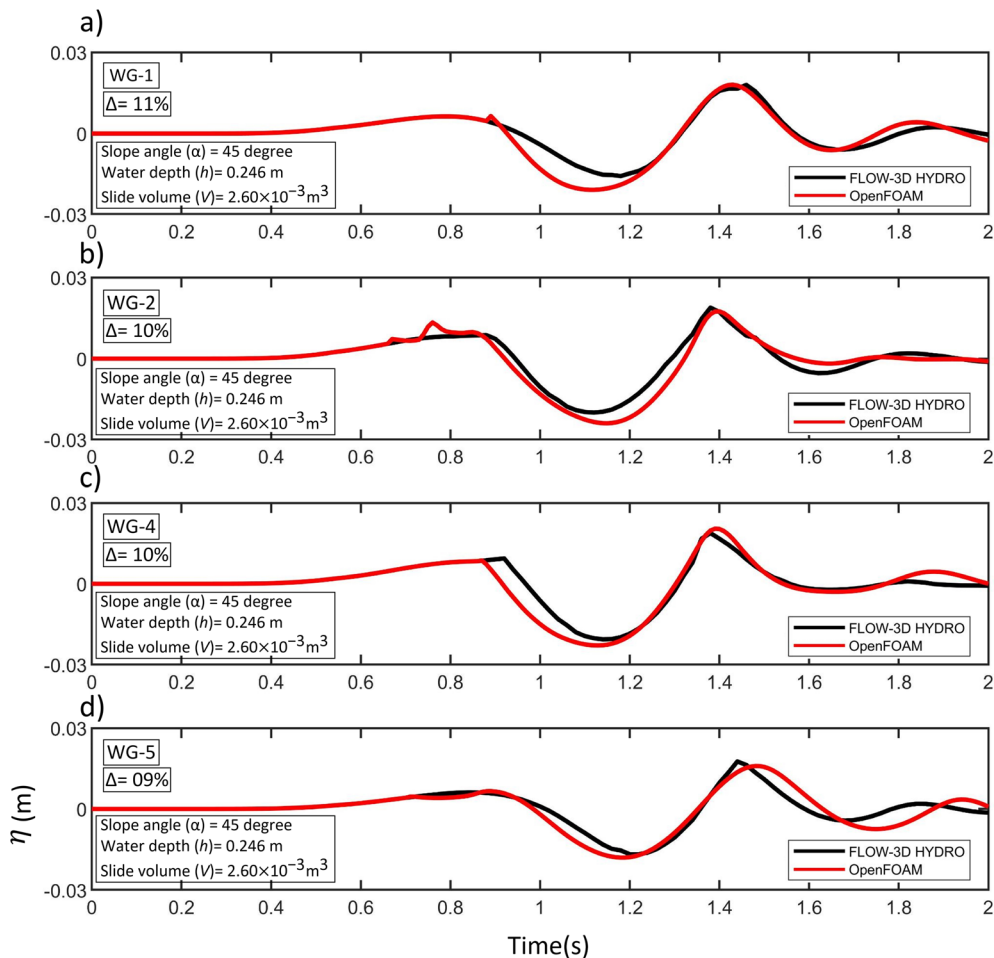

Figure 5
Comparison between the simulated waveforms by FLOW-3D HYDRO (black) and OpenFOAM (red) at four different locations in the near-field zone (WG-1,2,4 and 5). WG is the abbreviation for wave gauge. The mismatch (Δ) between the two models at each wave gauge is calculated using Eq. (14)
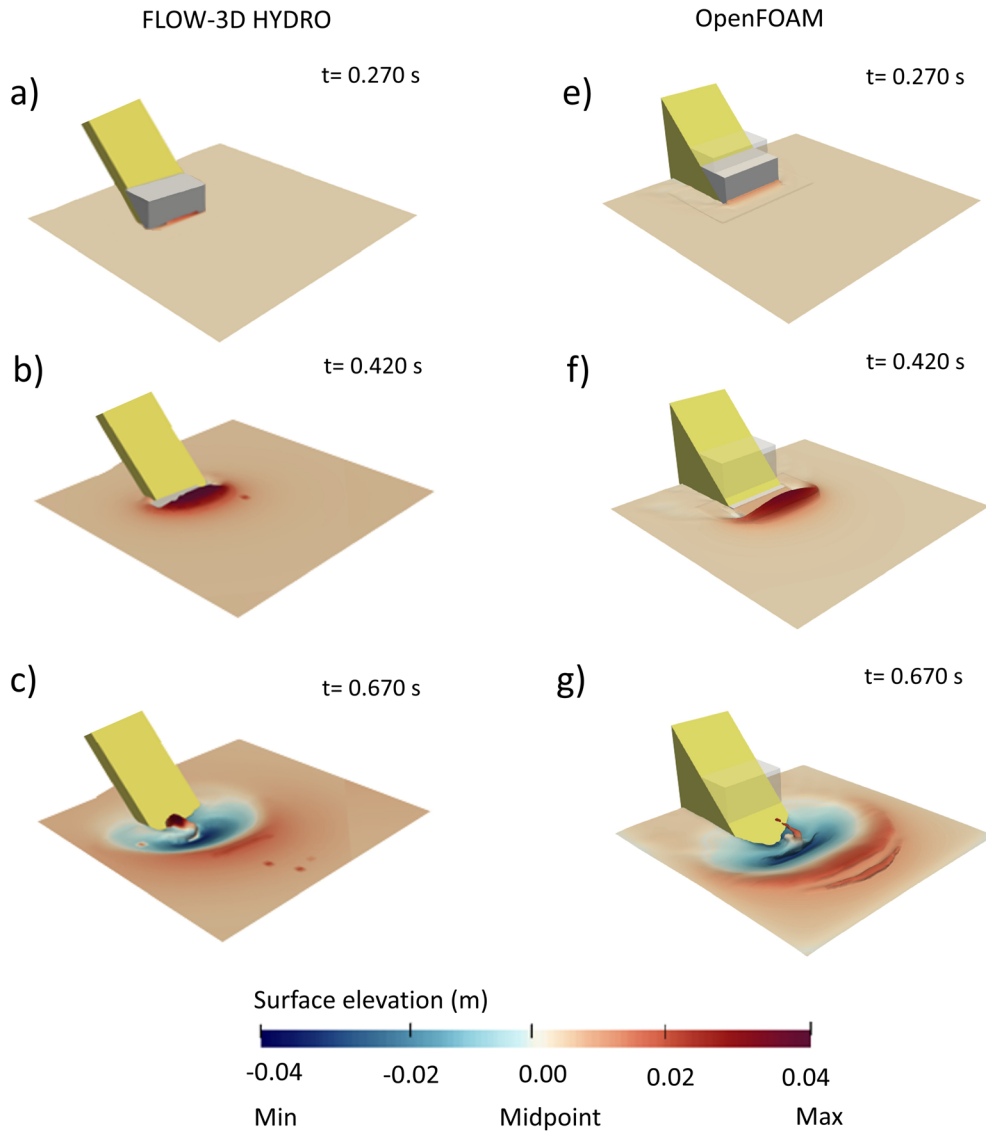
FLOW-3D HYDRO   OpenFOAM

Figure 6
Comparison of water surface elevations produced by solid-block subaerial landslides for the two numerical models FLOW-3D-HYDRO (**a–c**) and OpenFOAM (**e–g**) at different times

symmetry, and the other surfaces were of wall type with no-slip conditions around the walls.

To simulate turbulent flows, k-ω model was used because of its accuracy in modelling turbulent flows (Menter 1992). Landslide movement was replicated in simulations using coupled motion objects, which implies that the movement of landslides is based on gravity and the friction between surfaces rather than a specified motion in which the model should be

provided by force and torques. The time intervals of the numerical model outputs were set to 0.02 s to be consistent with the actual sampling rates of our wave gauges in the laboratory. In order to calibrate the FLOW-3D HYDRO model, the friction coefficient is set to 0.45, which is consistent with the Coulombic friction measurements in the laboratory. The Courant Number ($C = \frac{U\Delta t}{\Delta x}$) is considered as the criterion for the stability of numerical simulations which gives the
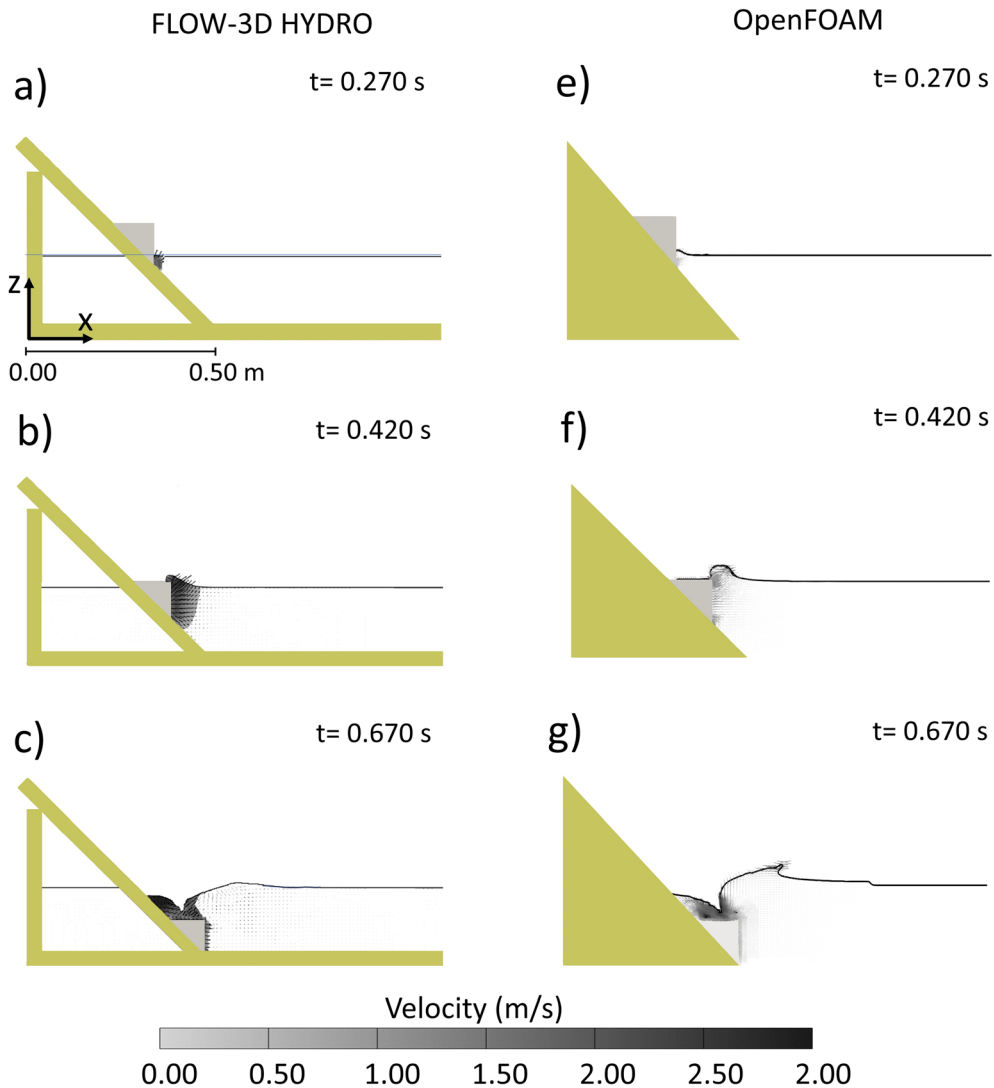
FLOW-3D HYDRO   OpenFOAM

Figure 7
Snapshots of the simulations at different times for FLOW-3D HYDRO (**a–c**) and OpenFOAM (**e–g**) showing velocity fields (colour maps and arrows). The colormaps indicate water particle velocity in m/s, and the lines indicate the velocities of water particles

maximum time step (Δt) for a prespecified mesh size (Δx) and flow speed (U). The Courant number was always kept below one.

2.2.3 OpenFOAM Simulation Procedure

OpenFOAM is an open-source platform containing several C^{++} libraries which solves both 3D Reynolds-Averaged Navier–Stokes equations (RANS) and Volume-Averaged RANS equations (VARANS) for two-phase flows (https://www.openfoam.com/documentation/user-guide). Its implementation is based on a tensorial approach using object-oriented programming techniques and the Finite Volume Method (McDonald 1971). In order to simulate the subaerial landslide-generated waves, the IHFOAM solver based on interFoam (Higuera et al., 2013a, 2013b), and the overset mesh framework method are employed. The implementation of the overset mesh method for porous mediums in
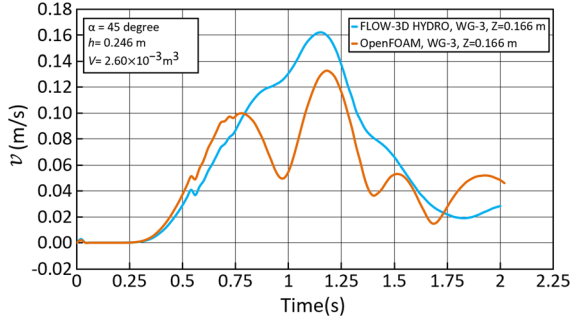
Figure 8

Comparison of velocity variations at (WG-3) for FLOW-3D HYDRO (light blue) and OpenFOAM (brown)

OpenFOAM is described in Romano et al. (2020a, b) for submerged rigid and impermeable landslides.

The overset mesh technique, as outlined by Romano et al. (2020a, b), uses two distinct domains: a moving domain that captures the dynamics of the rigid landslide and a static background domain to characterize the numerical wave tank. The overlapping of these domains results in a composite mesh that accurately depicts complex geometrical transformations while preserving mesh quality. A porous media with a very low permeability (n = 0.001) was used to simulate the impermeable sliding surfaces. RANS equations were solved within the porous media. The Multidimensional Universal Limiter with Explicit Solution (MULES) algorithm is employed for solving the (VOF) equation, ensuring precision in tracking fluid interfaces. Simultaneously, the PIMPLE algorithm is employed for the effective resolution of velocity–pressure coupling in the Eqs. 7 and 8. A background domain was created to reproduce the subaerial landslide waves with dimensions 2.50 m (x-direction) × 2.60 m (y-direction) × 0.6 m (z-direction) (Fig. 2c). The grid size is set to 0.005 m for the background mesh. A moving domain was applied in an area of 0.35 m (x-direction) × 0.46 m (y-direction) × 0.32 m (z-direction) with a grid spacing of 0.005 m and applying a body-fitted mesh approach, which contains the rigid and impermeable wedges. Wall condition with No-slip is defined as the boundary for the four side walls (left, right, front and back, in Fig. 1). Also, a non-slip boundary condition is specified to the bottom, whereas the top boundary is defined as open. The experimental slide movement time series is used to

model the landslide motion in OpenFOAM. The applied equation is based on the analytical solution by Pelinovsky and Poplavsky (1996) which was later elaborated by Watts (1998). The motion of a sliding rigid body is governed by the following equation:

$$(m + C_m m_0)\frac{d^2 s}{dt^2} = (m - m_0)g(sin\theta - C_n cos\theta)$$
$$- \frac{1}{2}C_d \rho A \left(\frac{ds}{dt}\right)^2 \qquad (12)$$

where, m represents the mass of the landslide, s is the displacement of the landslide down the slope, t is time elapsed, g stands for the acceleration due to gravity, θ is the slope angle, C_f is the Coulomb friction coefficient, C_m is the added mass coefficient, m_0 denotes the mass of the water displaced by the moving landslide, A is the cross-sectional area of the landslide perpendicular to the direction of motion, ρ is the water density, and C_d is the drag coefficient.

2.2.4 Mesh Sensitivity Analysis

In order to find the most efficient mesh size, mesh sensitivity analyses were conducted for both numerical models (Fig. 3). We considered the influence of mesh density on simulated waveforms by considering three mesh sizes (Δx) of 0.0025 m, 0.005 m and 0.010 m. The results of FLOW-3D HYDRO revealed that the largest mesh deviates 9% (Fig. 3a, Δx = 0.0100 m) from two other finer meshes. Since the simulations by FLOW-3D HYDRO for the finest mesh (Δx = 0.0025 m) do not show any improvements in comparison with the 0.005 m mesh, therefore the mesh with the size of Δx = 0.0050 m is used for simulations (Fig. 3a). A similar approach was followed for mesh sensitivity of OpenFOAM mesh grids. The mesh with the grid spacing of Δx = 0.0050 m was selected for further simulations since a satisfactory independence was observed in comparison with the half size mesh (Δx = 0.0025 m). However, results showed that the mesh size with the double size of the selected mesh (Δx = 0.0100 m) was not sufficiently fine to minimize the errors (Fig. 3b).

In terms of computational cost, the time required for 2 s simulations by FLOW-3D HYDRO is approximately 4.0 h on a PC Intel® Core™ i7-8700 CPU with a frequency of 3.20 GHz equipped with a 32 GB

RAM. OpenFOAM requires 20 h to run 2 s of numerical simulation on 2 processors on a PC Intel® Core™ i9-9900KF CPU with a frequency of 3.60 GHz equipped with a 364 GB RAM. Differences in computational time for simulations run with FLOW-3D HYDRO and OpenFOAM reflect the distinct characteristics of each numerical methods, and the specific hardware setups.

2.2.5 Validation

We validated both numerical models based on our laboratory experimental data (Fig. 4). The following criterion was used to assess the level of agreement between numerical simulations and laboratory observations:

$$\varepsilon = \left| \frac{Obs_i - Sim_i}{Obs_i} \right| \times 100 \tag{13}$$

where ε is the mismatch error, Obs_i is the laboratory observation values, Sim_i is the simulation values, and the mathematical expression $|X|$ represents the absolute value of X. The slope angle (α), water depth (h) and travel distance (D) were: $\alpha = 45°$, $h = 0.246$ m and $D = 0.045$ m in both numerical models, consistent with the physical model. We find the percentage error between each simulated data point and its corresponding observed value, and subsequently average these errors to assess the overall accuracy of the simulation against the observed time series. Our results revealed that the mismatch errors between physical experiments and numerical models for the FLOW-3D HYDRO and OpenFOAM are 8% and 18%, respectively, indicating that our models reproduce the measured waveforms satisfactorily (Fig. 4). The simulated waveform by OpenFOAM shows a minor mismatch at t = 0.76 s which resulted from a droplet immediately after the slide hits the water surface in the splash zone. In term of the maximum negative amplitude, the simulated waves by OpenFOAM indicates a relatively better performance than FLOW-3D HYDRO, whereas the maximum positive amplitude (a_M) simulated by FLOW-3D HYDRO is closer to the experimental value. The recorded maximum positive amplitude in physical experiment is 0.022 m, whereas it is 0.020 m for FLOW-3D HYDRO and

0.017 m for OpenFOAM simulations. In acknowledging the deviations observed, it is pertinent to highlight that while numerical models offer robust insights, the difference in meshing techniques and the distinct computational methods to resolve the governing equations in FLOW-3D HYDRO and OpenFOAM have contributed to the variance. Moreover, the intrinsic uncertainties associated with the physical experimentation process, including the precision of wave gauges and laboratory conditions, are non-negligible factors influencing the results.

3. Results

Following the validations of the two numerical models (FLOW-3D HYDRO and OpenFOAM), a series of simulations were performed to compare the performances of these two CFD solvers. The generation process of landslide waves, waveforms, and velocity fields are considered as the basis for comparing the performance of the two models (Figs. 5, 6, 7 and 8).

3.1. Comparison of Waveforms

Five numerical wave gauges were placed in our numerical models to measure water surface oscillations in the near-field zone (Fig. 5). These gauges offer an azimuthal coverage of 60° (Fig. 2d). Figure 5 reveals that the simulated waveforms from two models (FLOW-3D HYDRO and OpenFOAM) are similar. The highest wave amplitude (a_M) is recorded at WG-3 for both models, whereas the lowest amplitude is recorded at WG-5 and WG-1 which can be attributed to the longer distances of these gauges from the source region as well as their lateral offsets, resulting in higher wave energy dissipation at these gauges. The sharp peaks observed in the simulated waveforms, such as the red peak between 0.8–1.0 s in Fig. 5a from OpenFOAM, the red peak between 0.6–0.8 s in Fig. 5b also from OpenFOAM, and the black peak between 1.4–1.6 s in Fig. 5d from FLOW-3D HYDRO, are due to the models' spatial and temporal discretization. They reflect the sensitivity of the models to capturing transient phenomena, where the chosen mesh and time-

stepping intervals are key factors in the models' ability to track rapid changes in the flow field. To quantify the deviations of the two models from one another, we apply the following equation for mismatch calculation:

$$\Delta = \left| \frac{Sim_1 - Sim_2}{Sim_1} \right| \times 100 \qquad (14)$$

where Δ is the mismatch error, Sim_1 is the simulation values from FLOW-3D HYDRO, Sim_2 is the simulation values from OpenFOAM, and the mathematical expression $|X|$ implies the absolute value of X. We calculate the percentage difference for each corresponding pair of simulation results, then take the mean of these percentage differences to determine the average deviation between the two simulation time series. Using Eq. (14), we found a deviation range from 9 to 11% between the two models at various numerical gauges (Fig. 5), further confirming that the two models give similar simulation results.

3.2. Three-Dimensional Vision of Landslide Generation Process by Numerical Models

A sequence of four water surface elevation snapshots at different times is shown in Fig. 6 for both numerical modes. In both simulations, the sliding mass travels a constant distance of 0.045 m before hitting the water surface at t = 0.270 s which induces an initial change in water surface elevation (Figs. 6a and e). At t = 0.420 s, the mass is fully immersed for both simulations and an initial dipole wave is generated (Figs. 6b and f). Based on both numerical models, the maximum positive amplitude (0.020 m for FLOW-3D HYDRO, and 0.017 m for OpenFOAM) is observed at this stage (Fig. 6). The maximum propagation of landslide-simulated waves along with more droplets in the splash zone could be seen at t = 0.670 s for both models (Fig. 6c and g). The observed distinctions in water surface elevation simulations as illustrated in Fig. 6 are rooted in the unique computational methodologies intrinsic to each model. In the OpenFOAM simulations, a more diffused water surface elevation profile is evident. Such diffusion is an outcome of the simulation's intrinsic treatment of turbulent kinetic energy

dissipation, aligning with the solver's numerical dissipation characteristics. These traits are influenced by the selected turbulence models and the numerical advection schemes, which prioritize computational stability, possibly at the expense of interface sharpness. The diffusion in the wave pattern as rendered by OpenFOAM reflects the application of a turbulence model with higher dissipative qualities, which serves to moderate the energy retained during wave propagation. This approach can provide insights into the potential overestimation of energy loss under specific simulation conditions. In contrast, the simulations from FLOW-3D HYDRO depict a more localized wave pattern, indicative of a different approach to turbulent dissipation. This coherence in wave fronts is a function of the model's specific handling of the air–water interface and its targeted representation of the energy dynamics resulting from the landslide's interaction with the water body. They each have specific attributes that cater to different aspects of wave simulation fidelity, thereby contributing to a more comprehensive understanding of the phenomena under study.

3.3. Wave Velocity Analysis

We show four velocity fields at different times during landslide motion in Fig. 7 and one time series of velocity (Fig. 8) for both numerical models. The velocity varies in the range of 0–1.9 m/s for both models, and the spatial distribution of water particle velocity appears to be similar in both. The models successfully reproduce the complex wavefield around the landslide generation area, which is responsible for splashing water and mixing with air around the source zone (Fig. 7). The first snapshot at t = 0.270 s (Fig. 7a and e) shows the initial contact of the sliding mass with water surface for both numerical models which generates a small elevation wave in front of the mass exhibiting a water velocity of approximately 1.2 m/s. The slide fully immerses for the first time at t = 0.420 s producing a water velocity of approximately 1.5 m/s at this time (Fig. 7b and f). The last snapshot (t = 0.670 s) shows 1.20 s after the slide hits the bottom of the wave tank. Both models show similar patterns for the propagation of the waves towards the right side of the wave tank. The

differences in water surface profiles close to the slope and solid block at t = 0.67 s, observed in the FLOW-3D HYDRO and OpenFOAM simulations (Figs. 6 and 7), are due to the distinct turbulence models employed by each (RNG and k-ω SST, respectively) which handle the complex interactions of the landslide-induced waves with the structures differently. Additionally, the methods of simulating landslide movement further contribute to this discrepancy, with FLOW-3D HYDRO's coupled motion objects possibly affecting the waves' initiation and propagation unlike OpenFOAM's prescribed motion from experimental data. In addition to the turbulence models, the variations in VOF methodologies between the two models also contribute to the observed discrepancies.

For the simulated time series of velocity, both models give similar patterns and close maximum velocities (Fig. 8). For both models the WG-3 located at $X = 1.03$ m, $Y = 1.21$ m, and $Z = -0.55$ m (Fig. 2d) were used to record the time series. WG-3 is positioned 5 mm above the wave tank bottom, ensuring that the measurements taken reflect velocities very close to the bottom of the wave tank. The maximum velocity calculated by FLOW-3D HYDRO is 0.162 m/s while it is 0.132 m/s for OpenFOAM, implying a deviation of approximately 19% from one another. Some oscillations in velocity records are observed for both models, but these oscillations are clearer and sharper for OpenFOAM. Although it is hard to see velocity oscillations in the FLOW-3D HYDRO record, a close look may reveal some small oscillations (around t = 0.55 s and 0.9 s in Fig. 8). In fact, velocity oscillations are expected due to the variations in velocity of the sliding mass during the travel as well as due to the interferences of the initial waves with the reflected wave from the beach. In general, it appears that the velocity time series of the two models show similar patterns and similar maximum values although they have some differences in the amplitudes of the velocity oscillations. The differences between the two curves are attributed to factors such as difference in meshing between the two models, turbulence models, as well as the way that two models record the outputs.

4. Discussions

An important step for CFD modelling in academic or industrial projects is the selection of an appropriate numerical model that can deliver the task with satisfactory performance and at a reasonable computational cost. Obviously, the major drivers when choosing a CFD model are cost, capability, flexibility, and accessibility. In this sense, the existing options are of two types as follows:

- Commercial models, such as FLOW-3D HYDRO, which are optimised to solve free-surface flow problems, with customer support and an intuitive Graphical User Interface (GUI) that significantly facilitates meshing, setup, simulation monitoring, visualization, and post-processing. They usually offer high-quality customer support. Although these models show high capabilities and flexibilities for numerical modelling, they are costly, and thus less accessible.
- Open-source models, such as OpenFOAM, which come without a GUI but with coded tools for meshing, setup, parallel running, monitoring, post-processing, and visualization. Although these models offer no customer support, they have a big community support and online resources. Open-source models are free and widely accessible, but they may not be necessarily always flexible and capable.

OpenFOAM provides freedom for experimenting and diving through the code and formulating the problem for a user whereas FLOW-3D HYDRO comes with high-level customer supports, tutorial videos and access to an extensive set of example simulations (https://www.flow3d.com/). While FLOW-3D-HYDRO applies a semi-automatic meshing process where users only need to input the 3D model of the structure, OpenFOAM provides meshing options for simple cases, and in many advanced cases, users need to create the mesh in other software (e.g., ANSYS) (Ariza et al., 2018) and then convert it to OpenFOAM format. Auspiciously, there are numerous online resources (https://www.openfoam.com/trainings/about-trainings), and published examples for OpenFOAM (Rauter et al., 2021; Romano et al., 2020a, b; Zhang & Zhang, 2023).

The capabilities of both FLOW-3D HYDRO and OpenFOAM to simulate actual, complex landslide-generated wave events have been showcased in significant case studies. The study by Ersoy et al. (2022) applied FLOW-3D HYDRO to simulate impulse waves originating from landslides near an active fault at the Çetin Dam Reservoir, highlighting the model's capacity for detailed, site-specific modelling. Concurrently, the work by Alexandre Paris (2021) applied OpenFOAM to model the 2017 Karrat Fjord landslide tsunami events, providing a robust validation of OpenFOAM's utility in capturing the dynamics of real-world geophysical phenomena. Both instances exemplify the sophisticated computational approaches of these models in aiding the prediction and analysis of natural hazards from landslides.

As for limitations of this study, we acknowledge that our numerical models are validated by one real-world measured wave time series. However, it is believed that this one actual measurement was sufficient for validation of this study because it was out of the scope of this research to fully validate the FLOW-3D HYDRO and OpenFOAM models. These two models have been fully validated by more actual measurements by other researchers in the past (e.g., Sabeti & Heidarzadeh, 2022b). It is also noted that some of the comparisons made in this research were qualitative, such as the 3D wave propagation snapshots, as it was challenging to develop quantitative comparisons for snapshots. Another limitation of this study concerns the number of tests conducted here. We fixed properties such as water depth, slope angle, and travel distance throughout this study because it was out of the scope of this research to perform sensitivity analyses.

5. Conclusions

We configured, calibrated, validated and compared two numerical models, FLOW-3D HYDRO, and OpenFOAM, using physical experiments in a 3D wave tank. These validated models were used to simulate subaerial solid-block landslides in the near-field zone. Our results showed that both models are fully compatible with investigating waves generated by subaerial landslides, although they use different approaches to simulate the phenomenon. The properties of solid-block, water depth, slope angle, and travel distance were kept constant in this study as we focused on comparing the performance of the two models rather than conducting a full sensitivity analysis. The findings are as follows:

- Different settings were used in the two models for modelling landslide-generated waves. In terms of turbulent flow modelling, we used the Renormalization Group (RNG) turbulence model in FLOW-3D HYDRO, and k-ω (SST) turbulence model in OpenFOAM. Regarding meshing techniques, the overset mesh method was used in OpenFOAM, whereas the structured cartesian mesh was applied in FLOW-3D HYDRO. As for simulation of landslide movement, the coupled motion objects method was used in FLOW-3D HYDRO, and the experimental slide movement time series were prescribed in OpenFOAM.

- Our modelling revealed that both models successfully reproduced the physical experiments. The two models deviated 8% (FLOW-3D HYDRO) and 18% (OpenFOAM) from the physical experiments, indicating satisfactory performances. The maximum water particle velocity was approximately 1.9 m/s for both numerical models. When the simulated waveforms from the two numerical models are compared with each other, a deviation of 10% was achieved indicating that the two models perform approximately equally. Comparing the 3D snapshots of the two models showed that there are some minor differences in reproducing the details of the water splash in the near field.

- Regarding computational costs, FLOW-3D HYDRO was able to complete the same simulations in 4 h as compared to nearly 20 h by OpenFOAM. However, the hardware that were used for modelling were not the same; the computer used for the OpenFOAM model was stronger than the one used for running FLOW-3D HYDRO. Therefore, it is challenging to provide a fair comparison for computational time costs.

- Overall, we conclude that the two models give approximately similar performances, and they are both capable of accurately modelling landslide-

generated waves. The choice of a model for research or industrial projects may depend on several factors such as availability of local knowledge of the models, computational costs, accessibility and flexibilities of the model, and the affordability of the cost of a license (either a commercial or an open-source model).

Data Availability

All data used in this study are given in the body of the article. The data of landslide movement time series, and other details of this paper are available to public upon request to the corresponding author.

Declarations

Publisher's Note Springer Nature remains neutral with regard to jurisdictional claims in published maps and institutional affiliations.

References

Abadie, S., Morichon, D., Grilli, S., & Glockner, S. (2010). Numerical simulation of waves generated by landslides using a multiple-fluid Navier–Stokes model. *Coastal Engineering, 57*(9), 779–794. https://doi.org/10.1016/j.coastaleng.2010.04.002

Ariza, C., Casado, C., Wang, R.-Q., Adams, E., & Marugán, J. (2018). Comparative evaluation of OpenFOAM® and ANSYS® Fluent for the modeling of annular reactors. *Chemical Engineering & Technology, 41*(7), 1473–1483. https://doi.org/10.1002/ceat.201700455

Ataie-Ashtiani, B., & Najafi Jilani, A. (2007). A higher-order Boussinesq-type model with moving bottom boundary: Applications to submarine landslide tsunami waves. *Pure and Applied Geophysics, 164*(6), 1019–1048. https://doi.org/10.1002/fld.1354

Bayon, A., Valero, D., García-Bartual, R., & López-Jiménez, P. A. (2016). Performance assessment of OpenFOAM and FLOW-3D in the numerical modeling of a low Reynolds number hydraulic jump. *Environmental Modelling & Software, 80*, 322–335. https://doi.org/10.1016/j.envsoft.2016.02.018

Bellotti, G., & Romano, A. (2017). Wavenumber-frequency analysis of landslide-generated tsunamis at a conical island. Part II: EOF and modal analysis. *Coastal Engineering, 128*, 84–91. https://doi.org/10.1016/j.coastaleng.2017.07.008

Biscarini, C. (2010). Computational fluid dynamics modelling of landslide generated water waves. *Landslides, 7*(2), 117–124. https://doi.org/10.1007/s10346-009-0194-z

Brackbill, J. U., Kothe, D. B., & Zemach, C. (1992). A continuum method for modeling surface tension. *Journal of computational physics, 100*(2), 335–354.

Cecioni, C., Romano, A., Bellotti, G., Di Risio, M., & De Girolamo, P. (2011). Real-time inversion of tsunamis generated by

landslides. *Natural Hazards & Earth System Sciences, 11*(9), 2511–2520. https://doi.org/10.5194/nhess-11-2511-2011

Cremonesi, M., Frangi, A., & Perego, U. (2011). A Lagrangian finite element approaches the simulation of water-waves induced by landslides. *Computers & Structures, 89*(11–12), 1086–1093.

Del Jesus, M., Lara, J. L., & Losada, I. J. (2012). Three-dimensional interaction of waves and porous coastal structures: Part I: Numerical model formulation. *Coastal Engineering, 64*, 57–72. https://doi.org/10.1016/J.COASTALENG.2012.01.008

Di Risio, M., De Girolamo, P., Bellotti, G., Panizzo, A., Aristodemo, F., Molfetta, M. G., & Petrillo, A. F. (2009). Landslide-generated tsunamis runup at the coast of a conical island: New physical model experiments. *Journal of Geophysical Research: Oceans.* https://doi.org/10.1029/2008JC004858

Engelund, F., & Munch-Petersen, J. (1953). Steady flow in contracted and expanded rectangular channels. *La Houille Blanche*, (4), 464–481.

Ersoy, H., Oğuz Sünnetci, M., Karahan, M., & Perinçek, D. (2022). Three-dimensional simulations of impulse waves originating from concurrent landslides near an active fault using FLOW-3D software: A case study of Çetin Dam Reservoir (Southeast Turkey). *Bulletin of Engineering Geology and the Environment, 81*(7), 267. https://doi.org/10.1007/s10064-022-02675-8

Flow Science. (2022). *FLOW-3D HYDRO version 12.0 user's manual*. Santa Fe, NM, USA. Retrieved from https://www.flow3d.com/. 6 Aug 2023.

Fritz, H. M., Hager, W. H., & Minor, H. E. (2004). Near field characteristics of landslide generated impulse waves. *Journal of waterway, port, coastal, and ocean engineering, 130*(6), 287–302.

Fritz, H. M., Mohammed, F., & Yoo, J. (2009). Lituya bay landslide impact generated mega-tsunami 50th anniversary. In: *Tsunami science four years after the 2004 Indian Ocean Tsunami* (pp. 153–175). Birkhäuser Basel, Switzerland.

Grilli, S. T., Shelby, M., Kimmoun, O., Dupont, G., Nicolsky, D., Ma, G., Kirby, J. T., & Shi, F. (2017). Modelling coastal tsunami hazard from submarine mass failures: Effect of slide rheology, experimental validation, and case studies off the US East Coast. *Natural Hazards, 86*(1), 353–391. https://doi.org/10.1007/s11069-016-2692-3

Grilli, S. T., & Watts, P. (2005). Tsunami generation by submarine mass failure. I: Modelling, experimental validation, and sensitivity analyses. *Journal of Waterway, Port, Coastal, and Ocean Engineering, 131*(6), 283–297. https://doi.org/10.1061/(ASCE)0733-950X

Grilli, S. T., Zhang, C., Kirby, J. T., Grilli, A. R., Tappin, D. R., Watt, S. F. L., et al. (2021). Modeling of the Dec. 22nd, 2018, Anak Krakatau volcano lateral collapse and tsunami based on recent field surveys: Comparison with observed tsunami impact. *Marine Geology.* https://doi.org/10.1016/j.margeo.2021.106566

Heidarzadeh, M., Gusman, A., Ishibe, T., Sabeti, R., & Šepić, J. (2022). Estimating the eruption-induced water displacement source of the 15 January 2022 Tonga volcanic tsunami from tsunami spectra and numerical modelling. *Ocean Engineering, 261*, 112165. https://doi.org/10.1016/j.oceaneng.2022.112165

Heidarzadeh, M., Ishibe, T., Sandanbata, O., Muhari, A., & Wijanarto, A. B. (2020a). Numerical modeling of the *subaerial* landslide source of the 22 December 2018 Anak Krakatoa volcanic tsunami, Indonesia. *Ocean Engineering, 195*, 106733. https://doi.org/10.1016/j.oceaneng.2019.106733

Heidarzadeh, M., Putra, P. S., Nugroho, H. S., & Rashid, D. B. Z. (2020b). Field survey of tsunami heights and runups following the 22 December 2018 Anak Krakatau volcano tsunami, Indonesia. *Pure and Applied Geophysics, 177*, 4577–4595. https://doi.org/10.1007/s00024-020-02587-w

Heller, V., Bruggemann, M., Spinneken, J., & Rogers, B. D. (2016). Composite modelling of subaerial landslide–*tsunamis* in different water body geometries and novel insight into slide and wave kinematics. *Coastal Engineering, 109*, 20–41. https://doi.org/10.1016/j.coastaleng.2015.12.004

Heller, V., Hager, W. H., & Minor, H. E. (2008). Scale effects in subaerial landslide generated impulse waves. *Experiments in Fluids, 44*(5), 691–703. https://doi.org/10.1007/s00348-007-0427-7

Heller, V., & Spinneken, J. (2013). Improved landslide-tsunami prediction: Effects of block model parameters and *slide* model. *Journal of Geophysical Research: Oceans, 118*(3), 1489–1507. https://doi.org/10.1002/jgrc.20099

Higuera, P., Lara, J. L., & Losada, I. J. (2013a). Realistic wave generation and active wave absorption for Navier–Stokes models: Application to OpenFOAM®. *Coastal Engineering, 71*, 102–118. https://doi.org/10.1016/j.coastaleng.2012.07.002

Higuera, P., Lara, J. L., & Losada, I. J. (2013b). Simulating coastal engineering processes with OpenFOAM®. *Coastal Engineering, 71*, 119–134. https://doi.org/10.1016/j.coastaleng.2012.06.002

Hirt, C.W. and Nichols, B.D., 1981. Volume of fluid (VOF) method for the dynamics of free boundaries. *Journal of computational physics, 39*(1), 201–225.

Horrillo, J., Wood, A., Kim, G.-B., & Parambath, A. (2013). A simplified 3-D Navier–Stokes numerical model for landslide-tsunami: Application to the Gulf of Mexico. *Journal of Geophysical Research, 118*(12), 6934–6950. https://doi.org/10.1002/2012JC008689

Imamura, F., & Imteaz, M. A. (1995). Long waves in two-layers: Governing equations and numerical model. *Science of Tsunami Hazards, 13*(1), 3–24.

Jasak, H. (2009). OpenFOAM: Open source CFD in research and industry. *International Journal of Naval Architecture and Ocean Engineering, 1*(2), 89–94. https://doi.org/10.2478/IJNAOE-2013-0011

Kim, G. B., Cheng, W., Sunny, R. C., Horrillo, J. J., McFall, B. C., Mohammed, F., Fritz, H. M., Beget, J., & Kowalik, Z. (2020). Three-dimensional landslide generated tsunamis: Numerical and physical model comparisons. *Landslides, 17*(5), 1145–1161. https://doi.org/10.1007/s10346-019-01308-2

Kim, J., Pedersen, G. K., Løvholt, F., & LeVeque, R. J. (2017). A Boussinesq type extension of the GeoClaw model-a study of wave breaking phenomena applying dispersive long wave models. *Coastal Engineering, 122*, 75–86. https://doi.org/10.1016/j.coastaleng.2017.01.005

Kirby, J. T., Grilli, S. T., Horrillo, J., Liu, P. L. F., Nicolsky, D., Abadie, S., Ataie-Ashtiani, B., Castro, M. J., Clous, L., Escalante, C., Fine, I., et al. (2022). Validation and inter-comparison of models for landslide tsunami generation. *Ocean Modelling, 170*, 101943. https://doi.org/10.1016/j.ocemod.2021.101943

Lara, J. L., Ruju, A., & Losada, I. J. (2011). Reynolds averaged Navier–Stokes modelling of long waves induced by a transient wave group on a beach. *Proceedings of the Royal Society A: Mathematical, Physical and Engineering Sciences, 467*(2129), 1215–1242.

Larsen, B. E., & Fuhrman, D. R. (2018). On the over-production of turbulence beneath surface waves in Reynolds-averaged Navier–Stokes models. *Journal of Fluid Mechanics, 853*, 419–460.

Lee, C. H., & Huang, Z. (2021). Multi-phase flow simulation of impulsive waves generated by a sub-aerial granular landslide on an erodible slope. *Landslides, 18*(3), 881–895. https://doi.org/10.1007/s10346-020-01560-z

Liu, P. L. F., Woo, S. B., & Cho, Y. S. (1998). *Computer programs for tsunami propagation and inundation*. Technical Report. Cornell University, Ithaca, New York.

Liu, F., Wu, T.-R., Raichlen, F., Synolakis, C. E., & Borrero, J. C. (2005). Runup and rundown generated by three-dimensional sliding masses. *Journal of Fluid Mechanics, 536*(1), 107–144. https://doi.org/10.1017/S0022112005004799

Losada, I. J., Lara, J. L., & del Jesus, M. (2016). Modeling the interaction of water waves with porous coastal structures. *Journal of Waterway, Port, Coastal, and Ocean Engineering, 142*(6), 03116003

Løvholt, F., Harbitz, C. B., & Haugen, K. (2005). A parametric study of tsunamis generated by submarine slides in the Ormen Lange/Storegga area off western Norway. In: *Ormen Lange—An integrated study for safe field development in the Storegga submarine area* (pp. 219–231). Elsevier. https://doi.org/10.1016/B978-0-08-044694-3.50023-8

Løvholt, F., Bondevik, S., Laberg, J. S., Kim, J., & Boylan, N. (2017). Some giant submarine landslides do not produce large tsunamis. *Geophysical Research Letters, 44*(16), 8463–8472

Løvholt, F. J. M. R., Griffin, J., & Salgado-Gálvez, M. A. (2022). Tsunami hazard and risk assessment on the global scale. *Complexity in Tsunamis, Volcanoes, and their Hazards*, 213–246

Lynett, P., & Liu, P. L. F. (2005). A numerical study of the run-up generated by three-dimensional landslides. *Journal of Geophysical Research: Oceans*. https://doi.org/10.1029/2004JC002443

Lynett, P. J., & Martinez, A. J. (2012). A probabilistic approach for the waves generated by a submarine landslide. *Coastal Engineering Proceedings, 33*, 15–15. https://doi.org/10.9753/icce.v33.currents.15

McDonald, P. W. (1971). The computation of transonic flow through two-dimensional gas turbine cascades (Vol. 79825, p. V001T01A089). American Society of Mechanical Engineers

Menter, F. R. (1992). Improved two-equation k-omega turbulence models for aerodynamic flows (No. A-92183). https://ntrs.nasa.gov/citations/19930013620

Panizzo, A., De Girolamo, P., Di Risio, M., Maistri, A., & Petaccia, A. (2005). Great landslide events in Italian artificial reservoirs. *Natural Hazards and Earth System Sciences, 5*(5), 733–740. https://doi.org/10.5194/nhess-5-733-2005

Paris, A. (2021). *Comparison of landslide tsunami models and exploration of fields of application*. Doctoral dissertation, Université de Pau et des Pays de l'Adour.

Paris, A., Heinrich, P., & Abadie, S. (2021). Landslide tsunamis: Comparison between depth-averaged and Navier–Stokes models. *Coastal Engineering, 170*, 104022. https://doi.org/10.1016/j.coastaleng.2021.104022

Pelinovsky, E., & Poplavsky, A. (1996). Simplified model of tsunami generation by submarine landslides. *Physics and Chemistry of the Earth, 21*(1–2), 13–17. https://doi.org/10.1016/S0079-1946(97)00003-7

Rauter, M., Hoße, L., Mulligan, R. P., Take, W. A., & Løvholt, F. (2021). Numerical simulation of impulse wave generation by idealized landslides with OpenFOAM. *Coastal Engineering, 165*, 103815. https://doi.org/10.1016/j.coastaleng.2020.103815

Rauter, M., Viroulet, S., Gylfadóttir, S. S., Fellin, W., & Løvholt, F. (2022). Granular porous landslide tsunami modelling–the 2014 Lake Askja flank collapse. *Nature Communications, 13*(1), 678. https://doi.org/10.1038/s41467-022-28356-2

Romano, A., Bellotti, G., & Di Risio, M. (2013). Wavenumber–frequency analysis of the landslide-generated tsunamis at a conical island. *Coastal Engineering, 81*, 32–43. https://doi.org/10.1016/j.coastaleng.2013.06.007

Romano, A., Lara, J., Barajas, G., Di Paolo, B., Bellotti, G., Di Risio, M., Losada, I., & De Girolamo, P. (2020a). Tsunamis generated by submerged landslides: Numerical analysis of the near-field wave characteristics. *Journal of Geophysical Research: Oceans, 125*(7), e2020JC016157. https://doi.org/10.1029/2020JC016157

Romano, M., Ruggiero, A., Squeglia, F., Maga, G., & Berisio, R. (2020b). A structural view of SARS-CoV-2 RNA replication machinery: RNA synthesis, proofreading and final capping. *Cells*, 9(5), 1267.

Sabeti, R., & Heidarzadeh, M. (2022a). Numerical simulations of water waves generated by subaerial granular and solid-block landslides: Validation, comparison, and predictive equations. *Ocean Engineering, 266*, 112853. https://doi.org/10.1016/j.oceaneng.2022.112853

Sabeti, R., & Heidarzadeh, M. (2022b). Numerical simulations of tsunami wave generation by submarine landslides: Validation and sensitivity analysis to landslide parameters. *Journal of Waterway, Port, Coastal, and Ocean Engineering, 148*(2), 05021016. https://doi.org/10.1061/(ASCE)WW.1943-5460.0000694

Takabatake, T., Han, D. C., Valdez, J. J., Inagaki, N., Mäll, M., Esteban, M., & Shibayama, T. (2022). Three-dimensional physical modeling of tsunamis generated by partially submerged landslides. *Journal of Geophysical Research: Oceans, 127*(1), e2021JC017826. https://doi.org/10.1029/2021JC017826

Van Gent, M. R. A. (1995). Porous flows through rubble-mound material. *Journal of waterway, port, coastal, and ocean engineering, 121*(3), 176–181.

Wang, X., & Liu, P. L. F. (2006). An analysis of 2004 Sumatra earthquake fault plane mechanisms and Indian Ocean tsunami. *Journal of Hydraulic Research, 44*, 147–154. https://doi.org/10.1080/00221686.2006.9521671

Watts, P. (1998). Wavemaker curves for tsunamis generated by underwater landslides. *Journal of Waterway, Port, Coastal, and Ocean Engineering, 124*(3), 127–137. https://doi.org/10.1061/(ASCE)0733-950X(1998)124:3(127)

Yin, Y., Zhang, C., Imamura, F., Harris, J. C., & Li, Z. (2015). Numerical analysis on wave generated by the Qianjiangping landslide in Three Gorges Reservoir. *China. Landslides, 12*(2), 355–364. https://doi.org/10.1007/s10346-015-0564-7

Zaniboni, F., & Tinti, S. (2014). Numerical simulations of the 1963 Vajont landslide, Italy: application of 1D Lagrangian modelling. *Natural hazards, 70*, 567–592.

Zhang, C., & Zhang, M. (2023). Numerical investigation of solitary wave attenuation and mitigation caused by vegetation using OpenFOAM. *Coastal Engineering Journal, 65*(2), 198–216. https://doi.org/10.1080/21664250.2022.2163844

Three-Dimensional Simulations of Subaerial Landslide-Generated Waves